Two-body electrodisintegration of the three-nucleon bound state with Δ-isobar excitation

L. P. Yuan,[1,*] K. Chmielewski,[1] M. Oelsner,[1] P. U. Sauer,[1] and J. Adam, Jr.[2]
[1]*Institut für Theoretische Physik, Universität Hannover, D-30167 Hannover, Germany*
[2]*Nuclear Physics Institute, Academy of Sciences of Czech Republic, CZ-25068 Řež, Czech Republic*
(Received 21 August 2002; published 27 November 2002)

Electrodisintegration of the three-nucleon bound state with two-body final states is described. The description uses nucleon degrees of freedom extended to include the excitation of a single nucleon to a Δ isobar. The baryonic interaction and the electromagnetic current couple nucleonic states and states with a Δ isobar. Exact solutions of three-particle scattering equations are employed for the initial and final states of the reactions; due to the excitation of the Δ isobar an effective three-nucleon force is included. The current has one-baryon and two-baryon contributions. Theoretical predictions for the reactions with selected kinematic specifications are given. The role of the Δ isobar in the description of the considered processes is discussed and its effect on observables is quantitatively isolated.

DOI: 10.1103/PhysRevC.66.054004 PACS number(s): 21.45.+v, 25.30.Fj, 21.30.−x

I. INTRODUCTION

The concept of the spectral function for describing inelastic electron scattering from the three-nucleon bound state was developed in Ref. [1]. It was extended to include spin dependence in Ref. [2] and to include the Δ isobar degree of freedom in Ref. [3]. Restricting the electromagnetic (e.m.) nuclear current to its one-nucleon contribution, it was used for the description of inclusive electron scattering in different kinematic domains, i.e., in quasifree scattering [1,2], in the region of resonance pion production [4], and in deep-inelastic scattering [1,4,5]. The trinucleon spectral function was successful in accounting for the early inelastic scattering data of the three-nucleon bound state [1], and it was able to evaluate the experimental attempts of employing polarized ^{3}He as a substitute for a neutron spin target [2,4]. The spectral function contains compact information on the three-nucleon bound state, it is pictorial and therefore quite an appealing concept. However, it had always been realized that exclusive processes in inelastic electron scattering require a much more refined theoretical description, taking the hadronic final-state interaction as well as exchange currents fully into account, besides the one-nucleon current. That extension of the theory beyond the plane-wave impulse approximation with the spectral function had always been on our agenda it is now being done for excitation energies of final states well below the pion production threshold.

This paper reports on our description of two-body electrodisintegration of the three-nucleon bound state with the inclusion of final-state interaction and of exchange currents; the extension to three-body disintegration is in progress. Other groups [6–8] provided corresponding complete descriptions before us; especially the theoretical apparatus of Refs. [7,8] is quite comparable to ours. However, we add the Δ isobar as an active degree of freedom providing a mechanism for a three-nucleon force and for exchange currents.

We described radiative nucleon-deuteron capture and photodisintegration of the three-nucleon bound state with two-body final states in Refs. [9,10]. The description uses nucleon degrees of freedom extended to include the excitation of a single nucleon to a Δ isobar. The baryonic interaction and the e.m. current couple nucleonic states and states with a Δ isobar. Exact solutions of three-particle scattering equations [11–13] are employed for the initial and final states of the reactions. The effective three-nucleon force, mediated by the Δ isobar and consistent with the two-nucleon force, is included; it decreases the underbinding of the three-nucleon bound state, though it is unable to account for its binding in full. The current has one-baryon and two-baryon contributions; they are consistent with the interaction between the baryons. The paper applies the theoretical apparatus of Ref. [10] to the two-body electrodisintegration of the three-nucleon bound state. The role of the Δ isobar in the description of the considered e.m. reactions is discussed and found to be only moderately important for the studied observables.

This paper investigates trinucleon electrodisintegration with the same motivation as the corresponding photoreactions: Clear signatures for the need of a three-nucleon force and for the need of corresponding exchange currents, when theoretically describing the processes, are searched for and are hoped to be found. Compared with photoreactions, electrodisintegration is potentially even richer, since the momentum transfer carried out by the exchanged virtual photon is less constrained. Section II gives the calculational apparatus according to which the differential cross sections and spin observables of the considered processes are to be obtained.

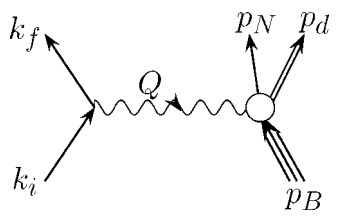

FIG. 1. Schematic description of two-body electrodisintegration of the three-nucleon bound state. Momenta are assigned to the particles involved. The lines for the two-baryon and three-baryon particles are drawn in a special form to indicate their compositeness.

*Electronic address: yuan@itp.uni-hannover.de

Section III presents selected results and Section IV our conclusions.

II. CALCULATIONAL SCHEME

The Hilbert space, the baryonic interaction, and the e.m. current are taken over from Ref. [10], where those calculational elements were used for the description of trinucleon photoreactions. In contrast to Ref. [10], the current operator has to carry an e.m. form factor, since the photon is virtual. To the extent to which it is possible, we also adopt the notation of Ref. [10]. Figure 1 shows the kinematics of the considered processes and defines the momenta of the particles involved; k_i and k_f are the electron four-momenta in the initial and final states, their rest mass being m_e; p_N, p_d, and p_B are the four-momenta of nucleon, deuteron, and trinucleon bound state, respectively, the corresponding rest masses being m_N, m_d, and m_B.

A. *S* matrix

We give various alternative forms for the *S*-matrix element connecting the prepared initial state $|i\boldsymbol{P}_i\rangle$ of initial momentum $\boldsymbol{P}_i$ with the final state $|f\boldsymbol{P}_f\rangle$ of final momentum $\boldsymbol{P}_f$:

$$\langle f\boldsymbol{P}_f|S|i\boldsymbol{P}_i\rangle=(-i)(2\pi\hbar)^4\delta(k_f+p_N+p_d-k_i-p_B)\langle s_f|M|s_i\rangle\frac{1}{(2\pi\hbar)^{15/2}}\frac{1}{\sqrt{2E_e(\boldsymbol{k}_i)2E_B(\boldsymbol{p}_B)2E_e(\boldsymbol{k}_f)2E_N(\boldsymbol{p}_N)2E_d(\boldsymbol{p}_d)}}, \tag{2.1a}$$

$$\langle f\boldsymbol{P}_f|S|i\boldsymbol{P}_i\rangle=\left(\frac{-i}{\hbar c}\right)\delta(k_f+p_N+p_d-k_i-p_B)\frac{1}{(2\pi)^2}\frac{1}{\sqrt{2E_e(\boldsymbol{k}_f)2E_e(\boldsymbol{k}_i)}}\frac{4\pi e_p^2}{(k_f-k_i)^2+io}\overline{u}(\boldsymbol{k}_f s_{e_f})\gamma_\mu u(\boldsymbol{k}_i s_{e_i})$$
$$\times\frac{1}{e_p c}\langle\psi_\alpha^{(-)}(\boldsymbol{q}_f)\nu_{\alpha_f}(Nd)|j^\mu(\boldsymbol{p}_N+\boldsymbol{p}_d-\boldsymbol{p}_B,\boldsymbol{p}_N+\boldsymbol{p}_d+\boldsymbol{p}_B)|B\mathcal{M}_{B_i}\rangle|_{\mathbf{q}_f=(\boldsymbol{p}_d-2\boldsymbol{p}_N)/3}. \tag{2.1b}$$

In Eq. (2.1b), $u(\boldsymbol{k}s)$ is the Dirac spinor of the electron with positive energy in the normalization $\overline{u}(\boldsymbol{k}s')u(\boldsymbol{k}s)=m_e c^2\delta_{s's}$; all other quantities, e.g., the initial trinucleon bound state $|B\mathcal{M}_{B_i}\rangle$ and the final nucleon-deuteron scattering state $|\psi_\alpha^{(-)}(\boldsymbol{q}_f)\nu_{\alpha_f}(Nd)\rangle$, are defined in Ref. [10]. $\langle s_f|M|s_i\rangle$ is the singularity-free matrix element for two-body electrodisintegration, from which the differential cross section

$$d\sigma=|\langle s_f|M|s_i\rangle|^2\frac{\mathrm{dLips}(k_i+p_B,k_f,p_N,p_d)}{4c^2\sqrt{(k_i\cdot p_B)^2-m_e^2m_B^2c^4}} \tag{2.2a}$$

is obtained. Its dependence on the spin projections s_{e_i} and $\mathcal{M}_{B_i}$ of electron and trinucleon bound state in the initial channel (collectively described by s_i), and on the spin projections s_{e_f}, m_{s_f}, and M_{I_f} of electron, nucleon, and deuteron in the final channel (collectively described by s_f), is explicitly indicated. $\langle s_f|M|s_i\rangle$ is defined by

$$\langle s_f|M|s_i\rangle=\frac{\hbar}{c}(2\pi\hbar)^{3/2}\frac{4\pi e_p^2}{(k_f-k_i)^2+io}\overline{u}(\boldsymbol{k}_f s_{e_f})\gamma_\mu u(\boldsymbol{k}_i s_{e_i})\sqrt{2E_N(\boldsymbol{p}_N)2E_d(\boldsymbol{p}_d)2E_B(\boldsymbol{p}_B)}$$
$$\times\frac{1}{e_p c}\langle\psi_\alpha^{(-)}(\boldsymbol{q}_f)\nu_{\alpha_f}(Nd)|j^\mu(\boldsymbol{p}_N+\boldsymbol{p}_d-\boldsymbol{p}_B,\boldsymbol{p}_N+\boldsymbol{p}_d+\boldsymbol{p}_B)|B\mathcal{M}_{B_i}\rangle|_{\mathbf{q}_f=(\boldsymbol{p}_d-2\boldsymbol{p}_N)/3} \tag{2.2b}$$

according to Eqs. (2.1). It is Lorentz invariant. The nuclear current

$$\sqrt{(E_N(\boldsymbol{p}_N)/m_Nc^2)(E_d(\boldsymbol{p}_d)/2m_Nc^2)}\langle\psi_\alpha^{(-)}(\boldsymbol{q}_f)\nu_{\alpha_f}(Nd)|$$
$$\times j^\mu(\boldsymbol{p}_N+\boldsymbol{p}_d-\boldsymbol{p}_B,\boldsymbol{p}_B)|B\mathcal{M}_{B_i}\rangle\sqrt{E_B(\boldsymbol{p}_B)/3m_Nc^2}$$

is a Lorentz vector; it contains our model assumptions on the three-baryon system, which is described in the framework of nonrelativistic quantum mechanics. Since the matrix element (2.2b) can be calculated in any frame, we choose the lab frame and adopt the following computational strategy:

(1) The experimental four-momentum transfer

$$Q=k_i-k_f, \tag{2.2c}$$

$$Q=p_N+p_d-p_B \tag{2.2d}$$

determines the total energy and the total momentum of the hadronic part of the system in the final channel. Measuring the direction of one momentum of the final two hadrons in

addition, i.e., $\hat{\boldsymbol{p}}_N$ or $\hat{\boldsymbol{p}}_d$, fixes both momenta $\boldsymbol{p}_N$ and $\boldsymbol{p}_d$ in full. This step is done using relativistic kinematics and the true experimental trinucleon mass.

(2) In contrast, all hadron energies, i.e., $E_N(\boldsymbol{p}_N)$, $E_d(\boldsymbol{p}_d)$, and $E_B(\boldsymbol{p}_B)$ involved in the matrix element (2.2b), are chosen non-relativistically and consistent with their -model values; here, the model trinucleon mass is used.

(3) Taking the model trinucleon binding energy for calculating the rest mass m_B and the average nucleon mass for the nucleon mass m_N, i.e., $m_N c^2 = 938.919$ MeV, the relative momentum $\boldsymbol{q}_f$ of the final nucleon-deuteron system is determined employing the nonrelativistic forms for the hadron energies, i.e.,

$$m_N c^2 + m_d c^2 + \boldsymbol{q}_f^2/(4m_N/3) + \boldsymbol{Q}^2/6m_N = m_B c^2 + Q^0 c.$$

Using the experimentally measured direction of the outgoing hadrons, i.e., $\hat{\boldsymbol{p}}_N$ or $\hat{\boldsymbol{p}}_d$, the magnitudes of $\boldsymbol{p}_N$ or $\boldsymbol{p}_d$ are determined nonrelativistically. Since nonrelativistic energy conservation is assumed and since the model trinucleon binding energy and therefore the trinucleon rest mass m_B are not the experimental ones, the resulting momenta $\boldsymbol{p}_N$ and $\boldsymbol{p}_d$ and the nucleon-deuteron energy do not have precisely the experimental values when calculating the matrix element $\langle s_f|M|s_i\rangle$.

(4) The electron will always be highly relativistic, i.e., its momentum is large compared with its rest mass, i.e., $m_e c \ll |\boldsymbol{k}_i|$, $m_e c \ll |\boldsymbol{k}_f|$, and $E_e(\boldsymbol{k}) = |\boldsymbol{k}| c$. However, the baryons can be considered to move nonrelativistically in the considered reactions, i.e., the calculational strategy for the matrix element $\langle s_f|M|s_i\rangle$ is physically sound.

The other building blocks for the differential cross section (2.2a) are the Lorentz-invariant phase-space element $\mathrm{dLips}(k_i + p_B, k_f, p_N, p_d)$, i.e.,

$$\begin{aligned}&\mathrm{dLips}(k_i + p_B, k_f, p_N, p_d)\\ &\quad = (2\pi\hbar)^4 \delta(k_f + p_N + p_d - k_i - p_B)\\ &\quad\times \frac{d^3k_f}{(2\pi\hbar)^3 2E_e(\boldsymbol{k}_f)} \frac{d^3p_N}{(2\pi\hbar)^3 2E_N(\boldsymbol{p}_N)} \frac{d^3p_d}{(2\pi\hbar)^3 2E_d(\boldsymbol{p}_d)},\end{aligned} \tag{2.3}$$

and the flux factor $4c^2\sqrt{(k_i \cdot p_B)^2 - m_e^2 m_B^2 c^4}$ containing information on the initial state. In contrast to the matrix element $\langle s_f|M|s_i\rangle$ which contains our model assumptions, the kinematic parts of the differential cross section, the Lorentz-invariant phase-space element and the flux factor, have to be calculated with the true experimental and relativistic energies of proton, deuteron, and ^{3}He for ^{3}He electrodisintegration. In contrast to our approach, Refs. [7,8] prefer a completely nonrelativistic description of the cross section (2.2a).

B. Polarization

We discuss the differential cross section for the following particular experimental situation. The three-nucleon target is in the lab system at rest; coordinate axes are defined to be

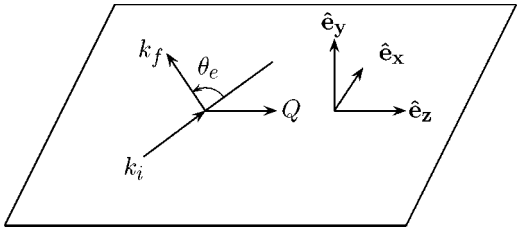

FIG. 2. Coordinate axes of the employed lab system. The scattering angle of the electron is denoted by θ_e.

$$\hat{\boldsymbol{e}}_z = \hat{\boldsymbol{Q}}, \tag{2.4a}$$

$$\hat{\boldsymbol{e}}_y = \frac{\hat{\boldsymbol{k}}_i \times \hat{\boldsymbol{k}}_f}{|\hat{\boldsymbol{k}}_i \times \hat{\boldsymbol{k}}_f|}, \tag{2.4b}$$

$$\hat{\boldsymbol{e}}_x = \hat{\boldsymbol{e}}_y \times \hat{\boldsymbol{e}}_z, \tag{2.4c}$$

i.e., the electron scattering plane is the x-z plane, $\boldsymbol{Q}$ the three-momentum transfer $\boldsymbol{Q} = \boldsymbol{k}_i - \boldsymbol{k}_f$ according to Eq. (2.2c), and $\hat{\boldsymbol{e}}_y$ is normal to the scattering plane. The chosen coordinate system is illustrated in Fig. 2. The incoming electron and the spin-$\frac{1}{2}$ three-nucleon target are assumed to be in pure polarized states. Since the electron is relativistic, only its longitudinal polarization needs to be considered, its four-dimensional polarization vector n_e being

$$n_e = h_e \frac{k_i}{m_e c}. \tag{2.5}$$

The possible polarization of the scattered electron will not be observed; thus, the differential cross section depends on the electron current tensor in the form

$$\begin{aligned}&L^{\mu\nu}(\boldsymbol{k}_f, \boldsymbol{k}_i; n_e)\\ &\quad = \sum_{s_{e_f}} [\overline{u}(\boldsymbol{k}_f s_{e_f}) \gamma^\mu u(\boldsymbol{k}_i n_e)]^* [\overline{u}(\boldsymbol{k}_f s_{e_f}) \gamma^\nu u(\boldsymbol{k}_i n_e)],\end{aligned} \tag{2.6a}$$

$$\begin{aligned}L^{\mu\nu}(\boldsymbol{k}_f, \boldsymbol{k}_i; n_e) = c^2[&(k_i + k_f)^\mu (k_i + k_f)^\nu - Q^\mu Q^\nu + g^{\mu\nu} Q^2\\ &+ 2ih_e \varepsilon^{\mu\nu\alpha\beta} k_{f\alpha} k_{i\beta}].\end{aligned} \tag{2.6b}$$

In Eq. (2.6a), $u(\boldsymbol{k}_i n_e)$ is a polarized Dirac spinor and $\varepsilon^{\mu\nu\alpha\beta}$ the totally antisymmetric tensor of four dimensions with $\varepsilon_{0123} = -\varepsilon^{0123} = 1$.

The three-nucleon target is at rest; its three-dimensional spin-polarized state $|n_B\rangle$ can therefore be expanded in terms of the two-dimensional Pauli spinors $|\mathcal{M}_B\rangle$ of the bound state $|B\mathcal{M}_B\rangle$. The polarization is defined by

$$\boldsymbol{\sigma}_B \hat{\boldsymbol{n}}_B |n_B\rangle = |n_B\rangle. \tag{2.7}$$

When the polarization is along a coordinate axis, the state $|n_B\rangle$ will be indicated by the corresponding unit vector, e.g.,

$|\hat{\boldsymbol{e}}_z\rangle$ for a state polarized along the z direction. The differential cross section depends on the nuclear current tensor in the form

$$
\begin{aligned}
&W^{\mu\nu}(\boldsymbol{p}_N\boldsymbol{p}_d\boldsymbol{p}_B;n_B)\\
&\quad=\frac{1}{e_p^2c^2}\,\frac{E_N(\boldsymbol{p}_N)}{m_Nc^2}\,\frac{E_d(\boldsymbol{p}_d)}{2m_Nc^2}\,\frac{E_B(\boldsymbol{p}_B)}{3m_Nc^2}\\
&\quad\times\sum_{\nu_{\alpha_f}}\langle\psi_\alpha^{(-)}(\boldsymbol{q}_f)\,\nu_{\alpha_f}(Nd)|j^\mu\\
&\quad\times(\boldsymbol{p}_N+\boldsymbol{p}_d-\boldsymbol{p}_B,\boldsymbol{p}_N+\boldsymbol{p}_d+\boldsymbol{p}_B)|Bn_B\rangle^*\\
&\quad\times\langle\psi_\alpha^{(-)}(\boldsymbol{q}_f)\,\nu_{\alpha_f}(Nd)|j^\nu\\
&\quad\times(\boldsymbol{p}_N+\boldsymbol{p}_d-\boldsymbol{p}_B,\boldsymbol{p}_N+\boldsymbol{p}_d+\boldsymbol{p}_B)|Bn_B\rangle. \qquad (2.8)
\end{aligned}
$$

The nuclear current tensor is defined for the particular experimental situation in which the bound state is polarized, but the spins of the hadrons in the final state, contained in the discrete quantum number ν_{α_f}, are not observed; the extension to more general spin observables of electrodisintegration can simply be done by a more general definition of the nuclear current tensor in Eq. (2.8).

C. Differential cross sections

The resulting differential cross section in the lab system is

$$
\begin{aligned}
&\frac{d^5\sigma(\boldsymbol{k}_i;h_en_B)}{dE_e(\boldsymbol{k}_f)d^2\hat{\boldsymbol{k}}_fd^2\hat{\boldsymbol{p}}_N}\\
&\quad=\sigma_{mott}\frac{1}{4E_e(\boldsymbol{k}_f)E_e(\boldsymbol{k}_i)/c^2\cos^2(\theta_e/2)}\\
&\quad\times\int d|\boldsymbol{p}_N|\boldsymbol{p}_N^2\delta[E_N(\boldsymbol{p}_N)+E_d(\boldsymbol{p}_d)\\
&\quad-Q_0c-m_Bc^2]\left[\frac{m_Nc^2}{E_N(\boldsymbol{p}_N)}\,\frac{2m_Nc^2}{E_d(\boldsymbol{p}_d)}\,\frac{3m_Nc^2}{m_Bc^2}\right.\\
&\quad\left.\times L_{\mu\nu}(\boldsymbol{k}_f,\boldsymbol{k}_i;h_e)W^{\mu\nu}(\boldsymbol{p}_N\boldsymbol{p}_d\boldsymbol{0};n_B)\right]\Bigg|_{\boldsymbol{p}_d=\boldsymbol{Q}-\boldsymbol{p}_N},
\end{aligned}
\qquad (2.9a)
$$

when the nucleon is observed, or

$$
\begin{aligned}
&\frac{d^5\sigma(\boldsymbol{k}_i;h_en_B)}{dE_e(\boldsymbol{k}_f)d^2\hat{\boldsymbol{k}}_fd^2\hat{\boldsymbol{p}}_d}\\
&\quad=\sigma_{mott}\frac{1}{4E_e(\boldsymbol{k}_f)E_e(\boldsymbol{k}_i)/c^2\cos^2(\theta_e/2)}\\
&\quad\times\int d|\boldsymbol{p}_d|\boldsymbol{p}_d^2\delta[E_N(\boldsymbol{p}_N)+E_d(\boldsymbol{p}_d)\\
&\quad-Q_0c-m_Bc^2]\left[\frac{m_Nc^2}{E_N(\boldsymbol{p}_N)}\,\frac{2m_Nc^2}{E_d(\boldsymbol{p}_d)}\,\frac{3m_Nc^2}{m_Bc^2}\right.\\
&\quad\left.\times L_{\mu\nu}(\boldsymbol{k}_f,\boldsymbol{k}_i;h_e)W^{\mu\nu}(\boldsymbol{p}_N\boldsymbol{p}_d\boldsymbol{0};n_B)\right]\Bigg|_{\boldsymbol{p}_N=\boldsymbol{Q}-\boldsymbol{p}_d},
\end{aligned}
\qquad (2.9b)
$$

when the deuteron is observed, with

$$
\sigma_{mott}=\left(\frac{e_p^2}{2E_e(\boldsymbol{k}_i)}\right)^2\frac{\cos^2(\theta_e/2)}{\sin^4(\theta_e/2)} \qquad (2.9c)
$$

being the Mott cross section. In Eqs. (2.9) the particle momenta and energies are the proper relativistic ones of the experiment; all model assumptions are confined to the nuclear current tensor W. The energy δ function can be integrated out analytically, which gives, besides energy conservation, the recoil factor

$$
\begin{aligned}
&\int d|\boldsymbol{p}_N|\boldsymbol{p}_N^2\delta[E_N(\boldsymbol{p}_N)+E_d(\boldsymbol{p}_d)-Q_0c-m_Bc^2]\\
&\quad=\left.\frac{|\boldsymbol{p}_N|E_N(\boldsymbol{p}_N)E_d(\boldsymbol{p}_d)/c^2}{E_d(\boldsymbol{p}_d)-E_N(\boldsymbol{p}_N)(\boldsymbol{p}_N\cdot\boldsymbol{p}_d)/\boldsymbol{p}_N^2}\right|_{\boldsymbol{p}_d=\boldsymbol{Q}-\boldsymbol{p}_N},
\end{aligned}
\qquad (2.10a)
$$

when the nucleon is observed, or

$$
\begin{aligned}
&\int d|\boldsymbol{p}_d|\boldsymbol{p}_d^2\delta[E_N(\boldsymbol{p}_N)+E_d(\boldsymbol{p}_d)-Q_0c-m_Bc^2]\\
&\quad=\left.\frac{|\boldsymbol{p}_d|E_N(\boldsymbol{p}_N)E_d(\boldsymbol{p}_d)/c^2}{E_N(\boldsymbol{p}_N)-E_d(\boldsymbol{p}_d)(\boldsymbol{p}_N\cdot\boldsymbol{p}_d)/\boldsymbol{p}_d^2}\right|_{\boldsymbol{p}_N=\boldsymbol{Q}-\boldsymbol{p}_d},
\end{aligned}
\qquad (2.10b)
$$

when the deuteron is observed. Energy conservation determines $|\boldsymbol{p}_N|$, when the nucleon is observed, and $|\boldsymbol{p}_d|$, when the deuteron is observed. In all kinematically allowed situations, there are one or two solutions for $|\boldsymbol{p}_N|$ or $|\boldsymbol{p}_d|$ for each given direction of the observed nucleon or deuteron; however, in all kinematic situations described in this paper, the solutions turn out to be unique for each measured direction or magnitude of the nucleon or deuteron. At the boundary of kinematically allowed regions, the recoil factors (2.10) become infinite [14]; at the same time the matrix elements are observed to tend to zero and the resulting cross sections remain smooth.

The contraction of the electron and nuclear current tensors $L\cdot W$ is needed for the differential cross sections (2.9) and is carried out in the Appendix. It is advantageous to define photon polarization four-vectors $\varepsilon(Q\lambda)$ assuming, without loss of generality, the coordinate system (2.4), i.e.,

$$
\varepsilon^\mu(Q\pm)=\mp\frac{1}{\sqrt{2}}(0,1,\pm i,0), \qquad (2.11a)
$$

$$\varepsilon^{\mu}(Q0)=\frac{1}{\sqrt{-Q^2}}(|\boldsymbol{Q}|,0,0,Q^0). \tag{2.11b}$$

$\lambda=+1,0,-1$ are the possible polarization values for a virtual photon. The polarization vectors satisfy $Q\cdot\varepsilon(Q\lambda)=0$; the other properties of the $\varepsilon(Q\lambda)$ are given and used in the Appendix. The contraction is carried out in the Appendix. After projecting the respective tensors on those polarization vectors, e.g.,

$$\begin{aligned}
&W(\boldsymbol{p}_N\boldsymbol{p}_d\boldsymbol{p}_B;n_B;\lambda\lambda')\\
&\quad=\frac{1}{e_p^2c^2}\frac{E_N(\boldsymbol{p}_N)}{m_Nc^2}\frac{E_d(\boldsymbol{p}_d)}{2m_Nc^2}\frac{E_B(\boldsymbol{p}_B)}{3m_Nc^2}\\
&\quad\times\sum_{\nu_{\alpha_f}}\langle\psi_{\alpha}^{(-)}(\boldsymbol{q}_f)\nu_{\alpha_f}(Nd)|j^{\mu}\\
&\quad\times(\boldsymbol{p}_N+\boldsymbol{p}_d-\boldsymbol{p}_B,\boldsymbol{p}_N+\boldsymbol{p}_d+\boldsymbol{p}_B)|Bn_B\rangle^*\varepsilon_{\mu}^*(Q\lambda')\\
&\quad\times\langle\psi_{\alpha}^{(-)}(\boldsymbol{q}_f)\nu_{\alpha_f}(Nd)|j^{\nu}(\boldsymbol{p}_N+\boldsymbol{p}_d-\boldsymbol{p}_B,\boldsymbol{p}_N+\boldsymbol{p}_d\\
&\quad+\boldsymbol{p}_B)|Bn_B\rangle\varepsilon_{\nu}(Q\lambda);
\end{aligned} \tag{2.12a}$$

all those tensor components are Lorentz scalars. Since according to Eq. (2.2d), the four-momentum transfer Q of the electron is also determined by the hadron momenta, the argument list of the nuclear current tensor does not have to be extended by Q. Furthermore, current conservation allows to replace the longitudinal current component by

$$\begin{aligned}
&\langle\psi_{\alpha}^{(-)}(\boldsymbol{q}_f)\nu_{\alpha_f}(Nd)|j^{\mu}(\boldsymbol{p}_N\\
&\quad+\boldsymbol{p}_d-\boldsymbol{p}_B,\boldsymbol{p}_N+\boldsymbol{p}_d+\boldsymbol{p}_B)|Bn_B\rangle\varepsilon_{\mu}(Q0)\\
&\quad=\sqrt{-\frac{Q^2}{\boldsymbol{Q}^2}}\langle\psi_{\alpha}^{(-)}(\boldsymbol{q}_f)\nu_{\alpha_f}(Nd)|j^0\\
&\quad\times(\boldsymbol{p}_N+\boldsymbol{p}_d-\boldsymbol{p}_B,\boldsymbol{p}_N+\boldsymbol{p}_d+\boldsymbol{p}_B)|Bn_B\rangle.
\end{aligned} \tag{2.12b}$$

In the final result, the longitudinal nuclear current components are replaced by charge components according to Eq. (2.12b), and the factor $\sqrt{-Q^2/\boldsymbol{Q}^2}$ is taken out of the current tensor; those modified tensor elements will be denoted by $W^{\lambda\lambda'}(\boldsymbol{p}_N\boldsymbol{p}_d\boldsymbol{p}_B;n_B)$ according to Eq. (A11) of the Appendix. By separating off the factor $\sqrt{-Q^2/\boldsymbol{Q}^2}$, the current components loose the property of being Lorentz scalars.

In terms of those current-tensor components $W^{\lambda\lambda'}(\boldsymbol{p}_N\boldsymbol{p}_d\boldsymbol{p}_B;n_B)$, the differential cross section in the lab system takes the final form,

$$\begin{aligned}
&\frac{d^5\sigma(\boldsymbol{k}_i;h_en_B)}{dE_e(\boldsymbol{k}_f)d^2\hat{\boldsymbol{k}}_fd^2\hat{\boldsymbol{p}}_N}\\
&\quad=\sigma_{mott}\int d|\boldsymbol{p}_N|\boldsymbol{p}_N^2\delta[E_N(\boldsymbol{p}_N)+E_d(\boldsymbol{p}_d)\\
&\quad-Q_0c-m_Bc^2]\frac{m_Nc^2}{E_N(\boldsymbol{p}_N)}\frac{2m_Nc^2}{E_d(\boldsymbol{p}_d)}\frac{3m_Nc^2}{m_Bc^2}\\
&\quad\times\Bigg[\sum_{\alpha}v_{\alpha}(Q\theta_e)R^{\alpha}(\boldsymbol{p}_N\boldsymbol{p}_d\boldsymbol{0};n_B)\\
&\quad+h_e\sum_{\alpha'}v_{\alpha'}(Q\theta_e)R^{\alpha'}(\boldsymbol{p}_N\boldsymbol{p}_d\boldsymbol{0};n_B)\Bigg]\Bigg|_{\boldsymbol{p}_d=\boldsymbol{Q}-\boldsymbol{p}_N},
\end{aligned} \tag{2.13a}$$

when the nucleon is observed, or

$$\begin{aligned}
&\frac{d^5\sigma(\boldsymbol{k}_i;h_en_B)}{dE_e(\boldsymbol{k}_f)d^2\hat{\boldsymbol{k}}_fd^2\hat{\boldsymbol{p}}_d}\\
&\quad=\sigma_{mott}\int d|\boldsymbol{p}_d|\boldsymbol{p}_d^2\delta[E_N(\boldsymbol{p}_N)+E_d(\boldsymbol{p}_d)-Q_0c\\
&\quad-m_Bc^2]\frac{m_Nc^2}{E_N(\boldsymbol{p}_N)}\frac{2m_Nc^2}{E_d(\boldsymbol{p}_d)}\frac{3m_Nc^2}{m_Bc^2}\\
&\quad\times\Bigg[\sum_{\alpha}v_{\alpha}(Q\theta_e)R^{\alpha}(\boldsymbol{p}_N\boldsymbol{p}_d\boldsymbol{0};n_B)\\
&\quad+h_e\sum_{\alpha'}v_{\alpha'}(Q\theta_e)R^{\alpha'}(\boldsymbol{p}_N\boldsymbol{p}_d\boldsymbol{0};n_B)\Bigg]\Bigg|_{\boldsymbol{p}_N=\boldsymbol{Q}-\boldsymbol{p}_d},
\end{aligned} \tag{2.13b}$$

when the deuteron is observed. The cross sections are simply derived from Eqs. (2.9), using the contraction $L\cdot W$ in the form of the Appendix. The $v_{\alpha}(Q\theta_e)$ and $v_{\alpha'}(Q\theta_e)$ are kinematic factors, whereas $R^{\alpha}(\boldsymbol{p}_N\boldsymbol{p}_d\boldsymbol{p}_B;n_B)$ and $R^{\alpha'}(\boldsymbol{p}_N\boldsymbol{p}_d\boldsymbol{p}_B;n_B)$ are the nuclear responses. The summation index α takes on the symbols L,T,TT, and TL; and α' takes the symbols T' and TL'; their significance will soon become obvious. The kinematic factors have the explicit forms

$$v_L(Q\theta_e)=\left(\frac{Q^2}{\boldsymbol{Q}^2}\right)^2, \tag{2.14a}$$

$$v_T(Q\theta_e)=-\frac{1}{2}\left(\frac{Q^2}{\boldsymbol{Q}^2}\right)+\tan^2(\theta_e/2), \tag{2.14b}$$

$$v_{TT}(Q\theta_e)=\frac{1}{2}\frac{Q^2}{\boldsymbol{Q}^2}, \tag{2.14c}$$

$$v_{TL}(Q\theta_e)=\frac{1}{\sqrt{2}}\left(\frac{Q^2}{\boldsymbol{Q}^2}\right)\sqrt{-\left(\frac{Q^2}{\boldsymbol{Q}^2}\right)+\tan^2(\theta_e/2)}, \tag{2.14d}$$

$$v_{T'}(Q\theta_e)=\sqrt{-\left(\frac{Q^2}{\boldsymbol{Q}^2}\right)+\tan^2(\theta_e/2)}\tan(\theta_e/2), \tag{2.14e}$$

$$v_{TL'}(Q\theta_e)=\frac{1}{\sqrt{2}}\left(\frac{Q^2}{\boldsymbol{Q}^2}\right)\tan(\theta_e/2), \tag{2.14f}$$

with θ_e being the scattering angle of the electron. The nuclear responses have the explicit forms,

$$R^L(\boldsymbol{p}_N\boldsymbol{p}_d\boldsymbol{p}_B;n_B)=W^{00}(\boldsymbol{p}_N\boldsymbol{p}_d\boldsymbol{p}_B;n_B), \tag{2.15a}$$

$$R^T(\boldsymbol{p}_N\boldsymbol{p}_d\boldsymbol{p}_B;n_B)=W^{++}(\boldsymbol{p}_N\boldsymbol{p}_d\boldsymbol{p}_B;n_B)+W^{--}(\boldsymbol{p}_N\boldsymbol{p}_d\boldsymbol{p}_B;n_B), \tag{2.15b}$$

$$R^{TT}(\boldsymbol{p}_N\boldsymbol{p}_d\boldsymbol{p}_B;n_B)=W^{+-}(\boldsymbol{p}_N\boldsymbol{p}_d\boldsymbol{p}_B;n_B)+W^{-+}(\boldsymbol{p}_N\boldsymbol{p}_d\boldsymbol{p}_B;n_B), \tag{2.15c}$$

$$R^{TL}(\boldsymbol{p}_N\boldsymbol{p}_d\boldsymbol{p}_B;n_B)=W^{0+}(\boldsymbol{p}_N\boldsymbol{p}_d\boldsymbol{p}_B;n_B)+W^{+0}(\boldsymbol{p}_N\boldsymbol{p}_d\boldsymbol{p}_B;n_B) - W^{0-}(\boldsymbol{p}_N\boldsymbol{p}_d\boldsymbol{p}_B;n_B)-W^{-0}(\boldsymbol{p}_N\boldsymbol{p}_d\boldsymbol{p}_B;n_B), \tag{2.15d}$$

$$R^{T'}(\boldsymbol{p}_N\boldsymbol{p}_d\boldsymbol{p}_B;n_B)=W^{++}(\boldsymbol{p}_N\boldsymbol{p}_d\boldsymbol{p}_B;n_B)-W^{--}(\boldsymbol{p}_N\boldsymbol{p}_d\boldsymbol{p}_B;n_B), \tag{2.15e}$$

$$R^{TL'}(\boldsymbol{p}_N\boldsymbol{p}_d\boldsymbol{p}_B;n_B)=W^{0+}(\boldsymbol{p}_N\boldsymbol{p}_d\boldsymbol{p}_B;n_B) + W^{+0}(\boldsymbol{p}_N\boldsymbol{p}_d\boldsymbol{p}_B;n_B)+W^{0-}(\boldsymbol{p}_N\boldsymbol{p}_d\boldsymbol{p}_B;n_B) + W^{-0}(\boldsymbol{p}_N\boldsymbol{p}_d\boldsymbol{p}_B;n_B). \tag{2.15f}$$

We use the convention of responses as given in Ref. [15]; alternatives are discussed in Ref. [16]. It can be read off from the definition of the nuclear responses that the response with superscript L refers to the longitudinal current component, T and T' to the same transverse current components, respectively, TT to the interference of different transverse current components, and TL and TL' to the interference of transverse and longitudinal current components. The responses with unprimed superscripts determine the cross sections for an unpolarized electron beam, those with primed superscripts are particular for the cross sections with polarized electron beams. Furthermore, the dependence on the nuclear polarization vector $\hat{\boldsymbol{n}}_B$ could be factored out, i.e.,

$$R^{\alpha}(\boldsymbol{p}_N\boldsymbol{p}_d\boldsymbol{p}_B;n_B)=R_0^{\alpha}(\boldsymbol{p}_N\boldsymbol{p}_d\boldsymbol{p}_B)+\hat{\boldsymbol{n}}_B\cdot\boldsymbol{R}^{\alpha}(\boldsymbol{p}_N\boldsymbol{p}_d\boldsymbol{p}_B), \tag{2.16a}$$

$$R^{\alpha'}(\boldsymbol{p}_N\boldsymbol{p}_d\boldsymbol{p}_B;n_B)=R_0^{\alpha'}(\boldsymbol{p}_N\boldsymbol{p}_d\boldsymbol{p}_B)+\hat{\boldsymbol{n}}_B\cdot\boldsymbol{R}^{\alpha'}(\boldsymbol{p}_N\boldsymbol{p}_d\boldsymbol{p}_B). \tag{2.16b}$$

The list of arguments used for the nuclear responses of Eqs. (2.15) and (2.16) is excessive; it is kept in order to make clear that the nuclear responses are determined solely by hadron properties. This paper calculates them in the lab system, i.e., for $\boldsymbol{p}_B=0$, and it chooses the coordinate system of Fig. 2. Respecting the energy conservation in the cross sections of Eqs. (2.13), the nuclear responses depend solely on the magnitude of the three-momentum transfer $|\boldsymbol{Q}|$ and on the direction of the observed nucleon or deuteron, i.e., on $(\theta_N\phi_N)$ or on $(\theta_d\phi_d)$. The paper describes in-plane experiments, i.e., ϕ_N and ϕ_d are 0 or π.

In contrast, when the description of out-of-plane experiments is attempted, the nuclear responses depend on ϕ_N or ϕ_d explicitly. That dependence is due to $\boldsymbol{q}_f=(\boldsymbol{p}_d-2\boldsymbol{p}_N)/3$ in the nuclear current matrix element $\langle\psi_\alpha^{(-)}(\boldsymbol{q}_f)\nu_{\alpha_f}(Nd)|j^\nu(\boldsymbol{p}_N+\boldsymbol{p}_d-\boldsymbol{p}_B,\boldsymbol{p}_N+\boldsymbol{p}_d+\boldsymbol{p}_B)|B\mathcal{M}_{B_i}\rangle\varepsilon_\nu(Q\lambda)$. Using the coordinate system of Fig. 2, the direction of $\boldsymbol{q}_f$ is described by the angles (θ,ϕ), with $\phi=\phi_N+\pi$, when the nucleon is observed, and $\phi=\phi_d$, when the deuteron is observed. In fact, the nuclear current matrix element depends on ϕ only through the phase factor $\exp[i(\mathcal{M}_{B_i}+\lambda-M_{I_f}-m_{s_f})\phi]$, i.e.,

$$\begin{aligned}&\langle\psi_\alpha^{(-)}(\boldsymbol{q}_f)\nu_{\alpha_f}(Nd)|j^\nu(\boldsymbol{p}_N+\boldsymbol{p}_d-\boldsymbol{p}_B,\boldsymbol{p}_N+\boldsymbol{p}_d+\boldsymbol{p}_B)|B\mathcal{M}_{B_i}\rangle\varepsilon_\nu(Q\lambda)\\&=\exp[i(\mathcal{M}_{B_i}+\lambda-M_{I_f}-m_{s_f})\phi]\times[\langle\psi_\alpha^{(-)}(\boldsymbol{q}_f)\nu_{\alpha_f}(Nd)|j^\nu(\boldsymbol{p}_N+\boldsymbol{p}_d-\boldsymbol{p}_B,\boldsymbol{p}_N+\boldsymbol{p}_d+\boldsymbol{p}_B)|B\mathcal{M}_{B_i}\rangle\varepsilon_\nu(Q\lambda)|_{\phi=0}],\end{aligned} \tag{2.17a}$$

$$\begin{aligned}&[\langle\psi_\alpha^{(-)}(\boldsymbol{q}_f)\nu_{\alpha_f}(-M_{I_f})(-m_{s_f})(Nd)|j^\nu\times(\boldsymbol{p}_N+\boldsymbol{p}_d-\boldsymbol{p}_B,\boldsymbol{p}_N+\boldsymbol{p}_d+\boldsymbol{p}_B)|\times B(-\mathcal{M}_{B_i})\rangle\varepsilon_\nu(Q-\lambda)|_{\phi=0}]\\&=(-1)^{1-M_{I_f}+(1/2)-m_{s_f}+1-\lambda+(1/2)-\mathcal{M}_{B_i}}\times[\langle\psi_\alpha^{(-)}(\boldsymbol{q}_f)\nu_{\alpha_f}M_{I_f}m_{s_f}|j^\nu(\boldsymbol{p}_N+\boldsymbol{p}_d-\boldsymbol{p}_B,\boldsymbol{p}_N+\boldsymbol{p}_d+\boldsymbol{p}_B)|B\mathcal{M}_{B_i}\rangle\varepsilon_\nu(Q\lambda)|_{\phi=0}].\end{aligned} \tag{2.17b}$$

Thus, the nuclear current matrix elements for out-of-plane experiments can easily be obtained from those with $\phi=0$ for in-plane experiments. In Eq. (2.17b) the spin projections M_{I_f} and m_{s_f} of the final state are made explicit for more transparency. Furthermore, if the trinucleon target is unpolarized, the dependence on ϕ can be separated off from the nuclear responses in a standard fashion, i.e.,

$$\frac{1}{2}\sum_{n_B}R^L(\boldsymbol{p}_N\boldsymbol{p}_d0;n_B)=r^L(|\boldsymbol{Q}|\theta_N), \tag{2.18a}$$

$$\frac{1}{2}\sum_{n_B}R^T(\boldsymbol{p}_N\boldsymbol{p}_d0;n_B)=r^T(|\boldsymbol{Q}|\theta_N), \tag{2.18b}$$

$$\frac{1}{2}\sum_{n_B}R^{TT}(\boldsymbol{p}_N\boldsymbol{p}_d0;n_B)=r^{TT}(|\boldsymbol{Q}|\theta_N)\cos(2\phi_N), \tag{2.18c}$$

$$\frac{1}{2}\sum_{n_B}R^{TL}(\boldsymbol{p}_N\boldsymbol{p}_d0;n_B)=r^{TL}(|\boldsymbol{Q}|\theta_N)\cos(\phi_N), \tag{2.18d}$$

$$\frac{1}{2}\sum_{n_B}R^{T'}(\boldsymbol{p}_N\boldsymbol{p}_d0;n_B)=0, \tag{2.18e}$$

$$\frac{1}{2}\sum_{n_B} R^{TL'}(\boldsymbol{p}_N\boldsymbol{p}_d 0;n_B)=r^{TL'}(|\boldsymbol{Q}|\theta_N)\sin(\phi_N), \tag{2.18f}$$

when the nucleon is observed. In Eqs. (2.18), (θ_N,ϕ_N) get replaced by (θ_d,ϕ_d), when the deuteron is observed. If the trinucleon target is unpolarized, a dependence on the electron beam polarization only survives for out-of-plane experiments. In the notation of Eqs. (2.16), the right-hand sides of Eqs. (2.18) correspond to $R_0^{\alpha}(\boldsymbol{p}_N\boldsymbol{p}_d 0)$ and $R_0^{\alpha'}(\boldsymbol{p}_N\boldsymbol{p}_d 0)$.

III. RESULTS

Calculations are performed for the reaction

$$e+{}^3\mathrm{He}\rightarrow e'+p+d \tag{3.1}$$

without polarization and for the reaction

$$\vec{e}+{}^3\vec{\mathrm{He}}\rightarrow e'+p+d \tag{3.2}$$

with specific polarizations. This paper considers experiments in which the observed proton or the observed deuteron are in the scattering plane; in those experiments, the unobserved hadron is also in the scattering plane.

The theoretical predictions are based on the baryonic interaction and the e.m. current of Ref. [10]. The purely nucleonic reference potential is the Paris potential [17]; it is extended to the coupled-channel potential $A2$ as in Ref. [18] to account for single Δ isobar excitation; two-body partial waves up to $I=2$ are taken into account. The trinucleon bound state and the scattering wave functions are computed and used for the reaction matrix element $\langle s_f|M|s_i\rangle$ as in Ref. [10]. The multipole expansion of the e.m. current is defined in Sec. A5 of Appendix A in Ref. [10]; charge, electric, and magnetic multipoles contribute; their highest multipole order to be considered is determined by the maximum three-baryon angular momentum $\mathcal{J}_{max}$ kept for the nucleon-deuteron scattering state. The calculations of this paper expand that scattering state up to $\mathcal{J}_{max}=21/2$, the highest multipole order therefore being 11. In contrast to Ref. [10] the current operator carries an e.m. form factor, since the photon is virtual; we choose the e.m. form factors of Ref. [19] for the nucleon; the relation between nucleon and Δ isobar form factors is taken from Ref. [20]. The calculations of the two-baryon current are marred by instabilities; those instabilities are dealt with as in Ref. [10], and they do not invalidate the numerical reliability of the obtained results. Furthermore, the calculations leave out the Coulomb interaction between the protons. Thus, the predictions are best suited for electrodisintegration of ^{3}H. However, the experimental data to which this paper compares its results will refer to ^{3}He.

The theoretical binding energy $m_Bc^2-3m_Nc^2$ is -7.702 MeV for the coupled-channel potential and -7.373 MeV for the Paris potential, the purely nucleonic reference potential, whereas the experimental binding energy is -7.718 MeV. Thus, the excitation energy of the final nucleon-deuteron system will only slightly deviate in the model calculations from its corresponding experimental value.

Our calculations of the Lorentz-invariant matrix element $\langle s_f|M|s_i\rangle$ of Eq. (2.2b) are frame dependent due to the use of nonrelativistic hadron dynamics; the degree of frame dependence represents the systematic theoretical error inherent in our calculations. We test the frame dependence by comparing results obtained in the lab, in the center-of-mass (c.m.), and in the Breit frames. The c.m. system is defined with respect to the momentum of the virtual photon, i.e., by $\boldsymbol{Q}+\boldsymbol{p}_B=0$, the final hadron state being in its c.m. system. The three calculations agree better than 2% for all observables discussed in this paper; the largest spread is for the spin observables of Fig. 14; they are very small in value and refer to the largest momentum transfer $|\boldsymbol{Q}|=621.6$ MeV/c considered. As usual, we trust the calculation in the Breit frame most, since then the hadron momenta, involved in the reaction, are smallest in the average. Nevertheless, in general we carry the calculation of $\langle s_f|M|s_i\rangle$ always out in the lab system, since that calculation is technically simplest for us. The frame dependence of the rather special spin observables will be explicitly shown further on in the context of Fig. 14. With respect to other observables, the discussion of this point is considered closed.

All existing data are obtained for the reaction (3.1) in Refs. [21–24]; they refer to the spin-averaged differential cross section,

$$\frac{d^5\sigma}{dE_e(\boldsymbol{k}_f)d^2\hat{\boldsymbol{k}}d^2\hat{\boldsymbol{p}}_N}=\frac{1}{4}\sum_{h_e=\pm1}\sum_{n_B}\frac{d^5\sigma(\boldsymbol{k}_i;h_e n_B)}{dE_e(\boldsymbol{k}_f)d^2\hat{\boldsymbol{k}}_f d^2\hat{\boldsymbol{p}}_N}, \tag{3.3}$$

when the nucleon is observed; when the deuteron is observed, $\hat{\boldsymbol{p}}_N$ is to be replaced by $\hat{\boldsymbol{p}}_d$. The comparison between data and theoretical predictions is done in Figs. 3–11. Spin observables of the reaction (3.2) are not measured yet; they will be measured in experiments planned at MIT/Bates and at JLab; we give examples for our predictions in Figs. 12–14.

Figures 3–5 refer to experiments without polarization in which the proton is observed. Figure 3 shows experimental data and theoretical predictions for the lab differential cross section at 367.1 MeV electron beam energy in the reaction kinematics $T1$ and $T2$, Fig. 4 at 390.0 MeV electron beam energy in the reaction kinematics $C1$, $C2$, and $C3$, and Fig. 5 at 390.0 MeV electron beam energy in the reaction kinematics HR. The data of Figs. 3–5 are taken from Ref. [21], where also the reaction kinematics are defined; their definitions are quoted in the figure captions. Figure 6 shows experimental data and theoretical predictions for the lab differential cross section at 527.9 MeV electron beam energy; the data are taken from Ref. [22]. The agreement between experimental data and theoretical prediction is mixed. The Δ isobar effect is moderate. It is split into detailed contributions in Fig. 7 for kinematics $T1$ at 367.1 MeV electron beam energy, shown in Fig. 3; it arises mostly from changes in the nucleonic part of the three-nucleon bound state due to

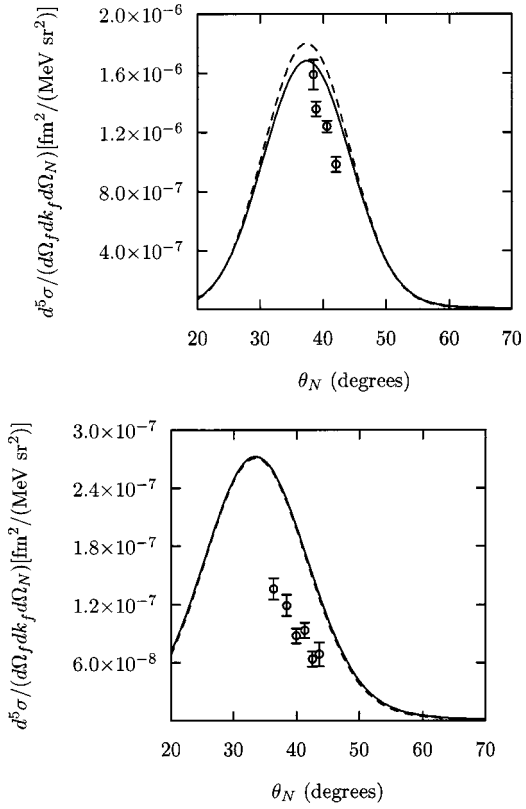

FIG. 3. Lab differential cross section of two-body electrodisintegration of ^{3}He at 367.1 MeV electron beam energy as a function of the proton lab angle θ_N with respect to the direction of the incoming electron. The data are taken from Ref. [21]. The plot on the top refers to the reaction kinematics $T1$, i.e., $\theta_e=85°$, $Q_0c=107.1$ MeV, and $|\boldsymbol{Q}|=431.0$ MeV/c, on the bottom it refers to the reaction kinematics $T2$, i.e., $\theta_e=85°$, $Q_0c=143.8$ MeV, and $|\boldsymbol{Q}|=412.7$ MeV/c. The full results for the interaction with Δ-isobar excitation are shown as solid lines, whereas the results for the purely nucleonic reference potential are shown as dashed lines. We note that the calculated nonrelativistic c.m. excitation energy of the final nucleon-deuteron system without rest masses, i.e., $e_d+3q_f^2/4m_N$, e_d being the deuteron binding energy, has the theoretical values 68.65 (68.98) MeV for the reaction kinematics $T1$ in the calculation with (without) Δ isobar, the discrepancy with the 68.63 MeV value arising from the proper experimental trinucleon binding energy is quite small. We see similarly extremely small discrepancies of the final-state excitation energy between theoretical prediction and experimental values in all other experiments of this paper, carried out and planned; we shall therefore not discuss this point any further.

the presence of the Δ isobar. Figures 8–11 refer to experiments [23,24] without polarization in which the deuteron is observed. The electron beam energies are 370 MeV and 576 MeV. Figure 8 shows results for parallel kinematics, i.e., for $\hat{\mathbf{p}}_d\|\hat{\mathbf{Q}}$, energy transfers, the electron scattering angle is varied and therefore θ_d as well, but the magnitude of the three-momentum transfer $|\boldsymbol{Q}|$ is kept fixed at $|\boldsymbol{Q}|=412$ MeV/c, 504 MeV/c, and 604 MeV/c. The cross sections are given as functions of the magnitude of the momentum $|\boldsymbol{p}_N|$ of the recoiling proton. Figure 9 shows results for different kinematic situations, but again the magnitude of the three-

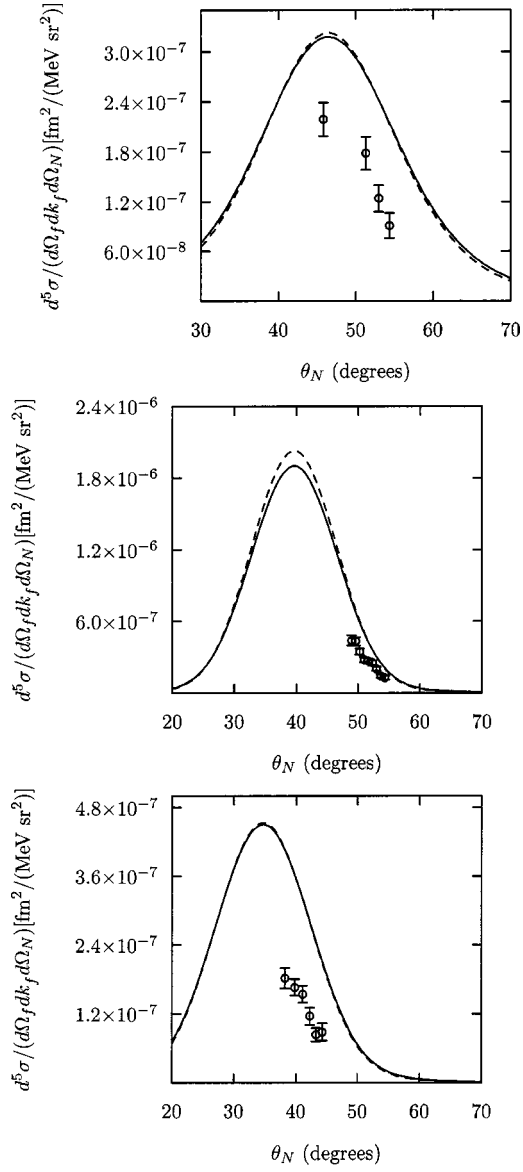

FIG. 4. Lab differential cross section of two-body electrodisintegration of ^{3}He at 390.0 MeV electron beam energy as a function of the proton lab angle θ_N with respect to the direction of the incoming electron. The data are taken from Ref. [21]. The plot on the top refers to the reaction kinematics $C1$, i.e., $\theta_e=74.4°$, $Q_0c=66.1$ MeV, and $|\boldsymbol{Q}|=434.8$ MeV/c; in the middle it refers to the reaction kinematics $C2$, i.e., $\theta_e=79.0°$, $Q_0c=110.4$ MeV, and $|\boldsymbol{Q}|=434.4$ MeV/c; and on the bottom it refers to the reaction kinematics $C3$, i.e., $\theta_e=83.0°$, $Q_0c=145.1$ MeV, and $|\boldsymbol{Q}|=434.5$ MeV/c. The full results for the interaction with Δ-isobar excitation are shown as solid lines, whereas the results for the purely nucleonic reference potential are shown as dashed lines.

momentum transfer $|\boldsymbol{Q}|$ is kept fixed at $|\boldsymbol{Q}|=412$ MeV/c, 504 MeV/c, and 604 MeV/c. The theoretical predictions overestimate the data, often by a factor of 2. The Δ isobar effect increases that discrepancy by about 10%; it gets more noticeable at larger nucleon momentum $|\boldsymbol{p}_N|$; both observations are somehow hidden by the logarithmic plots used in Refs. [23,24]. We note in passing that, according to more detailed calculations of ours, not reported on, the hadronic

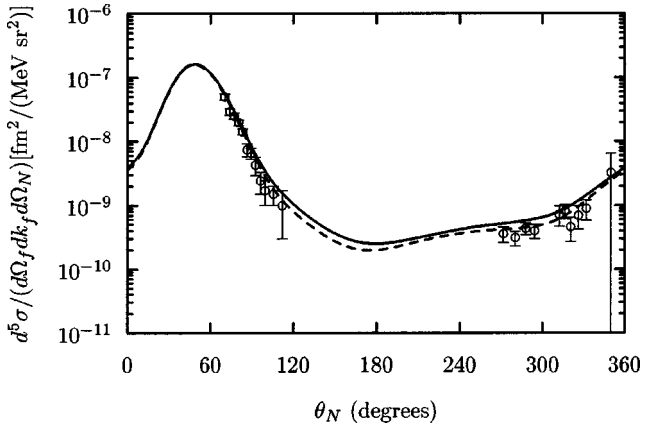

FIG. 5. Lab differential cross section of two-body electrodisintegration of ^{3}He at 390.0 MeV electron beam energy as a function of the proton lab angle θ_N with respect to the direction of the incoming electron. The data are taken from Ref. [21]. The plot refers to the reaction kinematics HR, i.e., $\theta_e = 39.7°$, $Q_0 c = 113.0$ MeV, and $|\boldsymbol{Q}| = 250.2$ MeV/c. The full results for the interaction with Δ-isobar excitation are shown as solid lines, whereas the results for the purely nucleonic reference potential are shown as dashed lines.

final state interaction shows up quite sizeably in the data, whereas the effect of meson exchange in the e.m. current is rather moderate. In Figs. 10 and 11 nuclear responses are extracted from the data and compared with theoretical predictions.

Third, we give theoretical predictions for selected spin observables of the reaction (3.2) with polarization. Experiments are planned [25] at MIT-Bates with beam energy 750 MeV. Experiments are also planned [25] at JLab with beam energy 2.4 GeV. The experiments will be done with a polarized beam and a target polarized in x and z directions of the

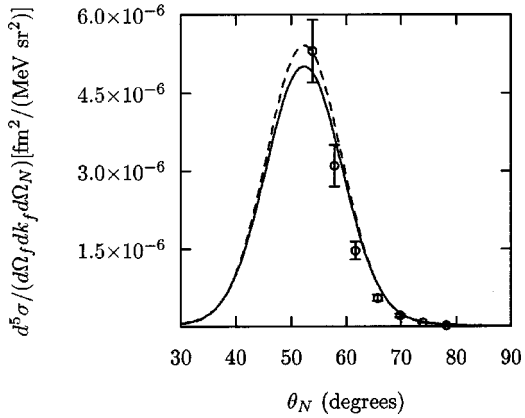

FIG. 6. Lab differential cross section of two-body electrodisintegration of ^{3}He at 527.9 MeV electron beam energy as a function of the proton lab angle θ_N with respect to the direction of the incoming electron. The data are taken from Ref. [22]. The plot refers to the reaction kinematics I, i.e., $\theta_e = 52.2°$, $Q_0 c = 99.8$ MeV, and $|\boldsymbol{Q}| = 430.0$ MeV/c. The full results for the interaction with Δ-isobar excitation are shown as solid lines, whereas the results for the purely nucleonic reference potential are shown as dashed lines.

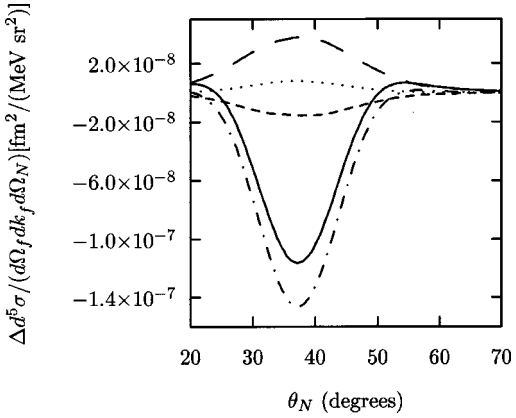

FIG. 7. Contribution to the Δ-isobar effect for the differential cross section of two-body electrodisintegration of ^{3}He as a function of the proton lab angle θ_N with respect to the direction of the incoming electron. The plot refers to 367.1 MeV electron beam energy with the reaction kinematics $T1$ of Ref. [21]. Shifts in the observable are shown. The full shift in the prediction, arising from the different predictions of the purely nucleonic reference potential and the coupled-channel potential, is shown as solid line. That full shift is split up into four distinct Δ contributions, i.e., the contribution arising from the theoretical change of the triton binding energy (dotted line), the contribution arising from the change of the nucleonic components in the bound-state wave function (dashed-dotted line), the contribution arising from the change of the nucleonic components in the scattering wave function (short-dashed line), and the contribution arising from the Δ components in both hadronic wave functions and from the e.m. current (long-dashed line); those four contributions add up to the full shift, making up the complete Δ-isobar effect.

scattering plane according to Fig. 2. They will measure the spin-averaged differential cross section and the asymmetries A_x and A_z, defined by

$$A_{x,z} = \left\{ \left[\frac{d^5\sigma(\boldsymbol{k}_i; h_e \hat{\boldsymbol{e}}_{x,z})}{dE_e(\boldsymbol{k}_f) d^2\hat{\boldsymbol{k}}_f d^2\hat{\boldsymbol{p}}_d} + \frac{d^5\sigma(\boldsymbol{k}_i; -h_e - \hat{\boldsymbol{e}}_{x,z})}{dE_e(\boldsymbol{k}_f) d^2\hat{\boldsymbol{k}}_f d^2\hat{\boldsymbol{p}}_d} \right] - \left[\frac{d^5\sigma(\boldsymbol{k}_i; h_e - \hat{\boldsymbol{e}}_{x,z})}{dE_e(\boldsymbol{k}_f) d^2\hat{\boldsymbol{k}}_f d^2\hat{\boldsymbol{p}}_d} + \frac{d^5\sigma(\boldsymbol{k}_i; -h_e \hat{\boldsymbol{e}}_{x,z})}{dE_e(\boldsymbol{k}_f) d^2\hat{\boldsymbol{k}}_f d^2\hat{\boldsymbol{p}}_d} \right] \right\} \Bigg/ \left\{ \left[\frac{d^5\sigma(\boldsymbol{k}_i; h_e \hat{\boldsymbol{e}}_{x,z})}{dE_e(\boldsymbol{k}_f) d^2\hat{\boldsymbol{k}}_f d^2\hat{\boldsymbol{p}}_d} + \frac{d^5\sigma(\boldsymbol{k}_i; -h_e - \hat{\boldsymbol{e}}_{x,z})}{dE_e(\boldsymbol{k}_f) d^2\hat{\boldsymbol{k}}_f d^2\hat{\boldsymbol{p}}_d} \right] + \left[\frac{d^5\sigma(\boldsymbol{k}_i; h_e - \hat{\boldsymbol{e}}_{x,z})}{dE_e(\boldsymbol{k}_f) d^2\hat{\boldsymbol{k}}_f d^2\hat{\boldsymbol{p}}_d} + \frac{d^5\sigma(\boldsymbol{k}_i; -h_e \hat{\boldsymbol{e}}_{x,z})}{dE_e(\boldsymbol{k}_f) d^2\hat{\boldsymbol{k}}_f d^2\hat{\boldsymbol{p}}_d} \right] \right\}. \quad (3.4)$$

For both planned experiments of reaction (3.2), predictions are available. We assume that the scattered electron at 750-MeV beam energy be observed under the angle $\theta_e = 30°$ with an energy loss $Q_0 c = 48$ MeV and a three-momentum transfer $|\boldsymbol{Q}| = 380$ MeV/c, and at 2.4-GeV beam energy under the angle $\theta_e = 15°$ with an energy loss $Q_0 c = 112.5$ MeV and a three-momentum transfer $|\boldsymbol{Q}| = 621.6$ MeV/c. In both experiments the magnitude of the proton recoil momentum centers around 20 MeV. For both experiments the c.m. exci-

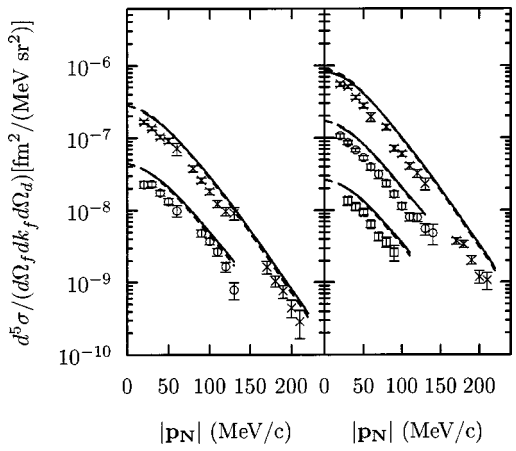

FIG. 8. Lab differential cross section of two-body electrodisintegration of ^{3}He as a function of the magnitude of the recoiling proton momentum $|\boldsymbol{p}_N|$. The left plot refers to 370 MeV electron beam energy and the right one to 576 MeV electron beam energy. Parallel kinematics, i.e. $\hat{\boldsymbol{p}}_d \| \hat{\boldsymbol{Q}}$, is assumed. The solid lines are obtained from a full coupled-channel calculation with the inclusion of single Δ-isobar excitation, and the dashed lines from a reference calculation without Δ-isobar excitation. The data are taken from Ref. [23]. They belong to three-momentum transfers 412 MeV/c (crosses), 504 MeV/c (open circles), and 604 MeV/c (open squares).

tation energy of the final nucleon-deuteron system is quite small; it stays below 40 MeV; the description of the final state in terms of nonrelativistic hadron dynamics is quite appropriate. We only show two spin observables for 2.4 GeV

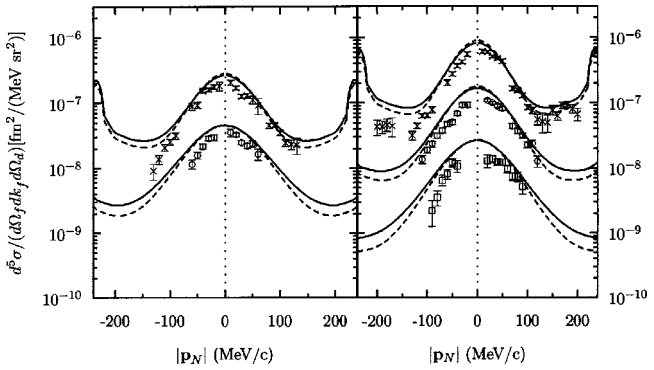

FIG. 9. Lab differential cross section of two-body electrodisintegration of ^{3}He as a function of the magnitude of the recoiling proton momentum $|\boldsymbol{p}_N|$. Negative $|\boldsymbol{p}_N|$ correspond to $\phi_d = \pi$. The left plot refers to 370 MeV electron beam energy and the right one to 576 MeV electron beam energy. The solid lines are obtained from a full coupled-channel calculation with the inclusion of single Δ-isobar excitation, the dashed lines from a reference calculation without Δ-isobar excitation. The data are taken from Ref. [24]. They belong to three-momentum transfers $|\boldsymbol{Q}|$/energy transfers Q_0 412/50 MeV/c (crosses), 504/70 MeV/c (open circles), and 604/100 MeV/c (open squares). At 370 MeV beam energy the electron scattering angles are 72.9° and 97.0°, at 576 MeV beam energy the electron scattering angles are 43.6°, 55.1°, and 69.3°, respectively, ordered according to increasing three-momentum transfer $|\boldsymbol{Q}|$.

electron beam energy. Sample spin observables are given as function of the direction θ_d of the deuteron in Figs. 12 and 13. The Δ-isobar effect can be sizable; it is split up into its detailed contributions and turns out to be a complicated superposition of several contributions. Figure 14 shows the frame dependence for the two spin observables especially studied: we note with concern, that the degree of frame dependence can be of the order of the Δ-isobar effect.

IV. CONCLUSIONS

The database for electrodisintegration with two-body final states is still rather small. All data known to us refer to in-plane processes without polarization. Striking disagreement between data and theoretical predictions is observed for the differential cross section in some particular kinematic regimes. We cannot relate that discrepancy yet to a definite shortcoming of the hadron dynamics and/or of the employed e.m. current on which the theoretical predictions rest.

We believe that the theoretical apparatus used is technically sound and physically quite realistic. In future, we shall use more modern and better calibrated two-nucleon potentials. Furthermore, we shall extend the calculations also to cover electrodisintegration of the three-nucleon bound state with three-nucleon final states.

ACKNOWLEDGMENTS

L.P.Y. was supported by DFG Grant No. Sa 247/25-1, and M. Oelsner by DFG Grant No. Sa 247/20-1/2. J.A. was supported by Grant No. GA CR 202/00/1669. The authors are grateful to their experimental colleagues S. Širca and Z.-L. Zhou for illuminating discussions. The calculations were performed at the Regionales Rechenzentrum für Niedersachen.

APPENDIX: CONTRACTION $L \cdot W$ OF ELECTRON AND NUCLEAR CURRENT TENSORS

The differential cross section (2.2a) depends on the square of the singularity-free matrix element $\langle s_f | M | s_i \rangle$ that is proportional to the contraction of the electron and nuclear current tensors,

$$L \cdot W = L_{\mu\nu}(\boldsymbol{k}_f, \boldsymbol{k}_i; n_e) W^{\mu\nu}(\boldsymbol{p}_N \boldsymbol{p}_d \boldsymbol{p}_B; n_B). \quad \text{(A1)}$$

This dependence is explicit in the forms (2.9) of the cross section. The contraction is calculated in this appendix. We use a method developed in Refs. [15,16].

The contraction (A1) is carried out by projecting both tensors on the photon polarization vectors $\varepsilon(Q\lambda)$ of Eq. (2.11a) using their property

$$\sum_\lambda (-1)^\lambda \varepsilon^{\mu *}(Q\lambda)\varepsilon^\nu(Q\lambda) = g^{\mu\nu} - Q^\mu Q^\nu / Q^2, \quad \text{(A2)}$$

with $Q = k_i - k_f = p_N + p_d - p_B$. Since the e.m. currents are conserved, the Lorentz-vector products of currents in the contraction can be replaced by products of components with respect to photon polarization vectors according to

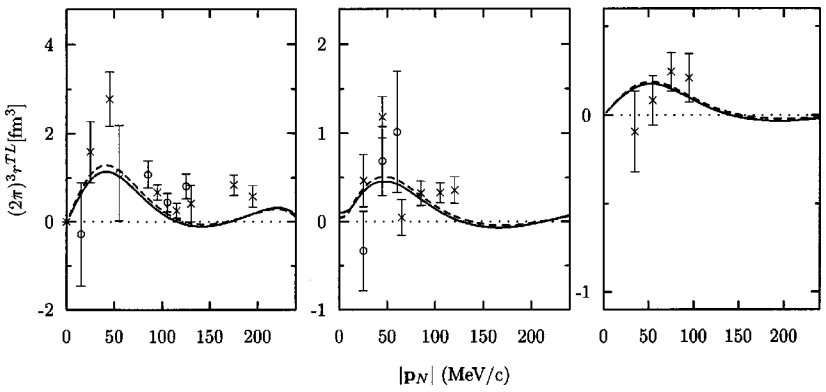

FIG. 10. Nuclear responses r^{TL} of two-body electrodisintegration of the unpolarized ^{3}He target as a function of the magnitude of the recoiling proton momentum $|\boldsymbol{p}_N|$. The dependence of r^{TL} on θ_d is transformed into the dependence on $|\boldsymbol{p}_N|$. The left plot refers to three-momentum transfer of 412 MeV/c, the middle one to 504 MeV/c, and the right one to 604 MeV/c. The solid lines are obtained from a full coupled-channel calculation with the inclusion of single Δ-isobar excitation, and the dashed lines from a reference calculation without Δ-isobar excitation. The data are taken from Ref. [24]; the open circles refer to 370 MeV electron beam energy and the crosses to the 576 MeV one.

$$\begin{aligned}\overline{u}(\boldsymbol{k}_f s_{ef})\gamma_\mu u(\boldsymbol{k}_i s_{ei})\langle \psi_\alpha^{(-)}(\boldsymbol{q}_f)\nu_{\alpha_f}(Nd)|&\\ \times j^\mu(\boldsymbol{p}_N+\boldsymbol{p}_d-\boldsymbol{p}_B,\boldsymbol{p}_N+\boldsymbol{p}_d+\boldsymbol{p}_B)|Bn_B\rangle&\\ =\sum_\lambda (-1)^\lambda[\overline{u}\boldsymbol{k}_f s_{ef})\gamma^\mu u(\boldsymbol{k}_i s_{ei})\varepsilon_\mu^*(Q\lambda)]&\\ \times[\langle \psi_\alpha^{(-)}(\boldsymbol{q}_f)\nu_{\alpha_f}(Nd)|j^\nu(\boldsymbol{p}_N+\boldsymbol{p}_d-\boldsymbol{p}_B,\boldsymbol{p}_N&\\ +\boldsymbol{p}_d+\boldsymbol{p}_B)|Bn_B\rangle\varepsilon_\nu(Q\lambda)].&\end{aligned} \tag{A3}$$

Thus, the contraction takes the alternative form

$$L\cdot W=\sum_{\lambda\lambda'}(-1)^{\lambda-\lambda'}L(\boldsymbol{k}_f,\boldsymbol{k}_i;n_e;\lambda\lambda')\times W(\boldsymbol{p}_N\boldsymbol{p}_d\boldsymbol{p}_B;n_B;\lambda\lambda'), \tag{A4}$$

with

$$L(\boldsymbol{k}_f,\boldsymbol{k}_i;n_e;\lambda\lambda')=\sum_{s_{ef}}[\overline{u}(\boldsymbol{k}_f s_{ef})\gamma^\mu u(\boldsymbol{k}_i n_e)]^*\varepsilon_\mu(Q\lambda')\times[\overline{u}(\boldsymbol{k}_f s_{ef})\gamma^\nu u(\boldsymbol{k}_i n_e)]\varepsilon_\nu^*(Q\lambda), \tag{A5a}$$

$$\begin{aligned}L(\boldsymbol{k}_f,\boldsymbol{k}_i;n_e;\lambda\lambda')=c^2[&(k_i+k_f)\cdot\varepsilon(Q\lambda')(k_i+k_f)\cdot\varepsilon^*(Q\lambda)\\ &+(-1)^\lambda\delta_{\lambda\lambda'}Q^2\\ &+2ih_e\varepsilon_{\mu\nu\alpha\beta}\varepsilon^\mu(Q\lambda')\varepsilon^{\nu*}(Q\lambda)k_f^\alpha k_i^\beta],\end{aligned} \tag{A5b}$$

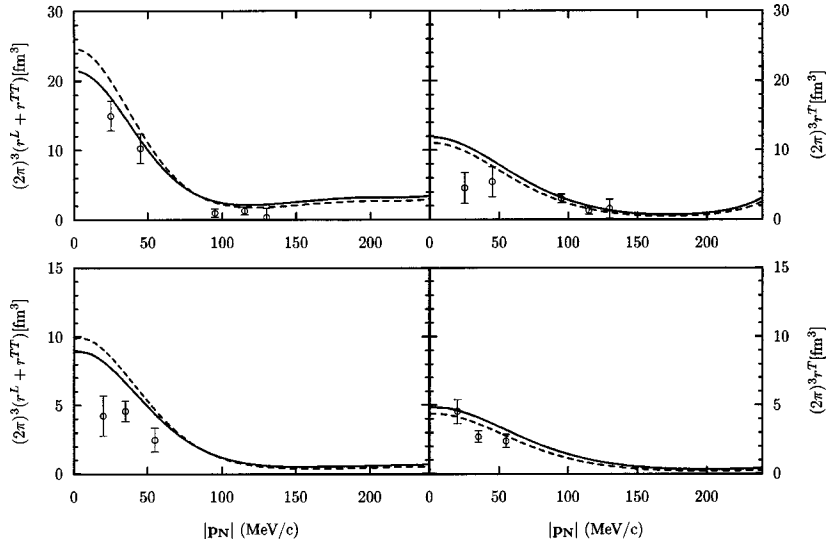

FIG. 11. Nuclear responses r^L+r^{TT} and r^T of two-body electrodisintegration of the unpolarized ^{3}He target as a function of the magnitude of the recoiling proton momentum $|\boldsymbol{p}_N|$. The dependence of r^{TL} on θ_d is transformed into the dependence on $|\boldsymbol{p}_N|$. The left plot refers to three-momentum transfer of 412 MeV/c, the middle one to 504 MeV/c, and the right one to 604 MeV/c. The solid lines are obtained from a full coupled-channel calculation with the inclusion of single Δ-isobar excitation, and the dashed lines from a reference calculation without Δ-isobar excitation. The data are taken from [24]; they refer to 370 MeV electron beam energy.

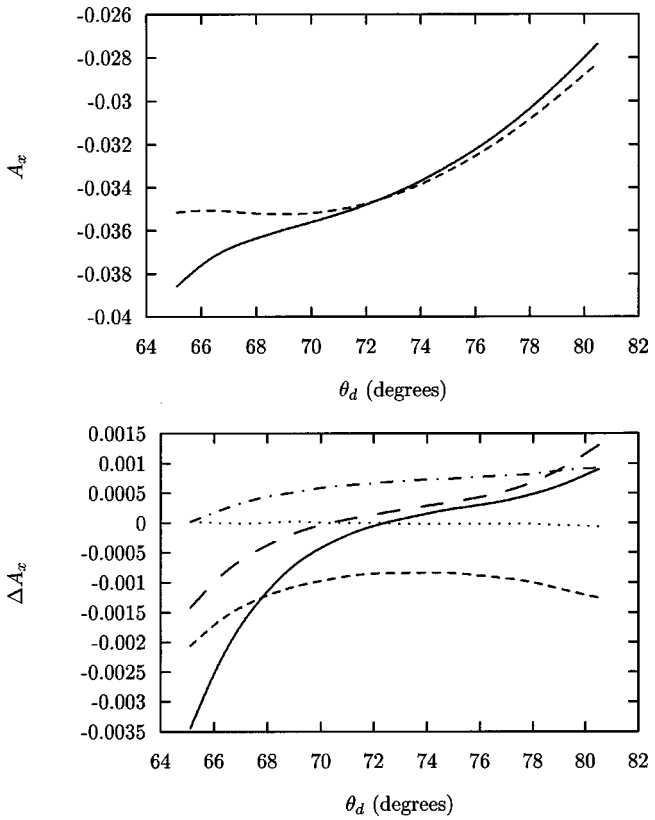

FIG. 12. Asymmetry A_x of two-body electrodisintegration of ^{3}He as a function of the deuteron lab angle θ_d with respect to the direction of the incoming electron. The plot refers to 2.4 GeV electron beam energy with the reaction kinematics defined in the text. In the top part, the full result for the interaction with Δ-isobar excitation is shown as solid line, whereas the result for the purely nucleonic reference potential is shown as a dashed line. In the bottom part, the Δ-isobar effect to the asymmetry A_z is studied in detail. Shifts in the observable are shown. The meaning of the different shifts and of the corresponding lines is the same as in Fig. 7.

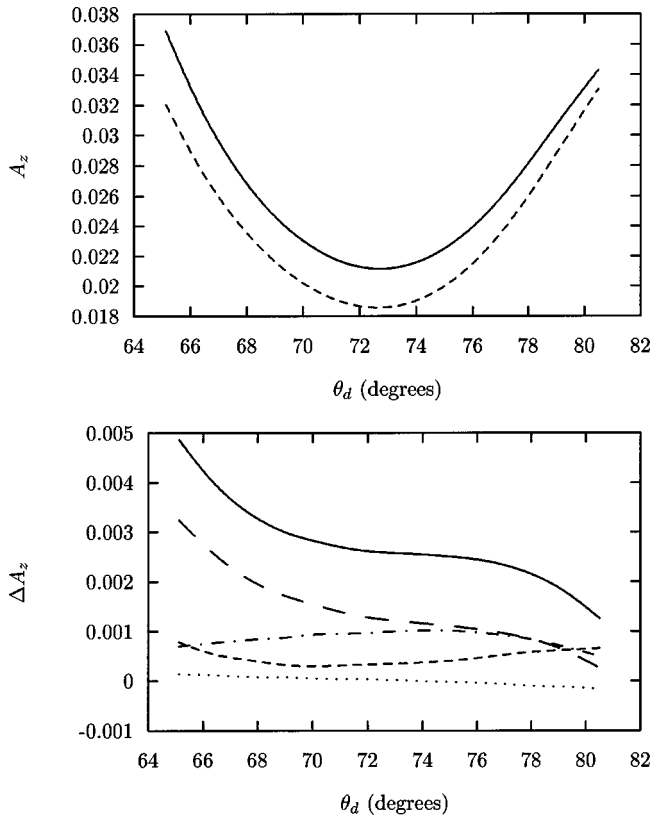

FIG. 13. Asymmetry A_z of two-body electrodisintegration of ^{3}He as a function of the deuteron lab angle θ_d with respect to the direction of the incoming electron. The plot refers to 2.4 GeV electron beam energy, with the reaction kinematics defined in the text. In the top part the full result for the interaction with Δ-isobar excitation is shown as a solid line, whereas the result for the purely nucleonic reference potential is shown as a dashed line. In the bottom part the Δ-isobar effect to the asymmetry A_z is studied in detail. Shifts in the observable are shown. The meaning of the different shifts and of the corresponding lines is the same as in Fig. 7.

$$L(\boldsymbol{k}_f,\boldsymbol{k}_i;n_e;\lambda\lambda')=L^0(\boldsymbol{k}_f,\boldsymbol{k}_i;n_e;\lambda\lambda')+h_eL^h(\boldsymbol{k}_f,\boldsymbol{k}_i;n_e;\lambda\lambda'), \quad \text{(A5c)}$$

and with $W(\boldsymbol{p}_N\boldsymbol{p}_d\boldsymbol{p}_B;n_B;\lambda\lambda')$ defined in Eq. (2.12a). In the remainder of this appendix we omit the momentum and polarization arguments in the current tensors for brevity. The current tensors of the $(\lambda\lambda')$ form satisfy the following symmetry relations:

$$L^0(\lambda\lambda')=L^0(\lambda'\lambda)^*, \quad \text{(A6a)}$$

$$L^0(-\lambda-\lambda')=(-1)^{\lambda-\lambda'}L^0(\lambda\lambda')^*, \quad \text{(A6b)}$$

$$L^h(\lambda\lambda')=L^h(\lambda'\lambda)^*, \quad \text{(A6c)}$$

$$L^h(-\lambda-\lambda')=(-1)^{1+\lambda-\lambda'}L^h(\lambda\lambda')^*, \quad \text{(A6d)}$$

and

$$W(\lambda\lambda')=W(\lambda'\lambda)^*. \quad \text{(A7)}$$

Thus, the electron current tensor has only six independent components, i.e., $L^0(00)$, and

$$L^0(0+)=-L^0(0-)^*=-L^0(-0)=L^0(+0)^*, \quad \text{(A8a)}$$

$$L^0(++)=L^0(--)^*, \quad \text{(A8b)}$$

$$L^0(+-)=L^0(-+)^*, \quad \text{(A8c)}$$

$$L^h(0+)=L^h(0-)^*=L^h(-0)=L^h(+0)^*, \quad \text{(A8d)}$$

$$L^h(++)=-L^h(--)^*, \quad \text{(A8e)}$$

with $L^h(00)=L^h(+-)=L^h(-+)=0$. The elements of the $(\lambda\lambda')$ tensors $L(\lambda\lambda')$ and $W(\lambda\lambda')$ are Lorentz scalars and can be calculated in any Lorentz frame. In the frame of Fig. 2 the components of the electron current tensor have the explicit forms

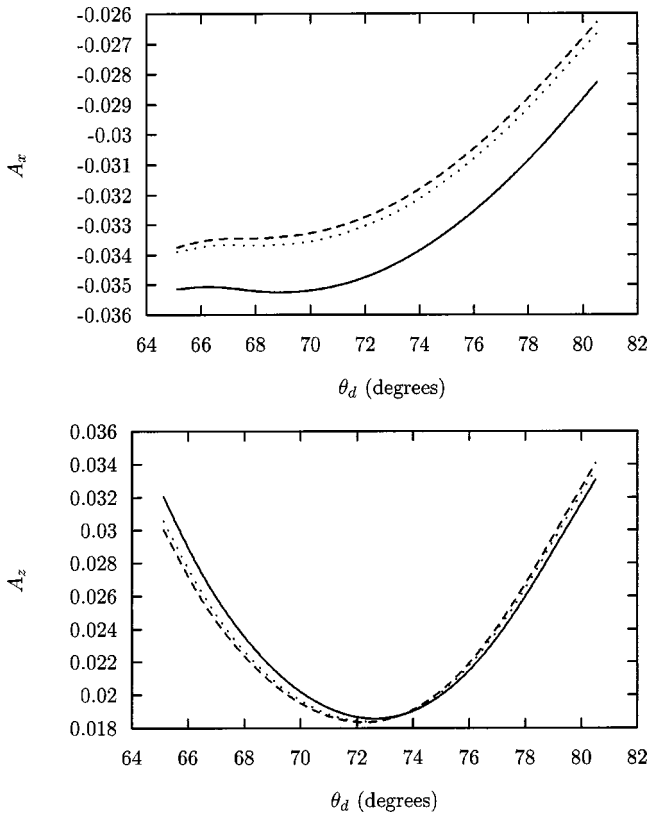

FIG. 14. Asymmetries A_x (top) and asymmetry A_z (bottom) of two-body electrodisintegration of ^{3}He as a function of the deuteron lab angle θ_d with respect to the direction of the incoming electron. The plot refers to 2.4 GeV electron beam energy with the reaction kinematics defined in the text. The results are for the purely nucleonic reference potential. The solid lines are results in the lab system, the dashed lines in the c.m. system, and the dotted lines in the Breit system.

$$L^0(00)=v_0\left[-\frac{Q^2}{\boldsymbol{Q}^2}\right], \tag{A9a}$$

$$L^0(0+)=v_0\frac{\sqrt{2}}{2}\frac{\sqrt{-Q^2}}{|\boldsymbol{Q}|}\sqrt{\tan^2(\theta_e/2)-\frac{Q^2}{\boldsymbol{Q}^2}}, \tag{A9b}$$

$$L^0(++)=v_0\left[\frac{-Q^2}{2\boldsymbol{Q}^2}+\tan^2(\theta_e/2)\right], \tag{A9c}$$

$$L^0(+-)=v_0\left[\frac{Q^2}{2\boldsymbol{Q}^2}\right], \tag{A9d}$$

$$L^h(0+)=v_0\frac{1}{\sqrt{2}}\frac{\sqrt{-Q^2}}{|\boldsymbol{Q}|}\tan(\theta_e/2), \tag{A9e}$$

$$L^h(++)=v_0\tan(\theta_e/2)\sqrt{\tan^2(\theta_e/2)-\frac{Q^2}{\boldsymbol{Q}^2}}, \tag{A9f}$$

with

$$v_0=\frac{4E_e(\boldsymbol{k}_f)E_e(\boldsymbol{k}_i)}{c^2}\cos^2(\theta_e/2). \tag{A9g}$$

All components of the electron current tensor turn out to be real. With those components the contraction $L\cdot W$ takes the following form:

$$\begin{aligned}L\cdot W=&v_0\left[-\frac{Q^2}{\boldsymbol{Q}^2}\right]W(00)+v_0\left[\frac{-Q^2}{2\boldsymbol{Q}^2}+\tan^2(\theta_e/2)\right]\\&\times[W(++)+W(--)]+v_0\left[\frac{Q^2}{2\boldsymbol{Q}^2}\right]\\&\times[W(+-)+W(-+)]\\&-v_0\frac{\sqrt{2}}{2}\frac{\sqrt{-Q^2}}{|\boldsymbol{Q}|}\sqrt{\tan^2(\theta_e/2)-\frac{Q^2}{\boldsymbol{Q}^2}}\\&\times[W(0+)+W(+0)-W(0-)-W(-0)]\\&+h_ev_0\tan(\theta_e/2)\sqrt{\tan^2(\theta_e/2)-\frac{Q^2}{\boldsymbol{Q}^2}}\\&\times[W(++)-W(--)]-h_ev_0\frac{1}{\sqrt{2}}\frac{\sqrt{-Q^2}}{|\boldsymbol{Q}|}\tan(\theta_e/2)\\&\times[W(0+)+W(+0)+W(0-)+W(-0)].\end{aligned} \tag{A10}$$

Finally, we rewrite certain components of the nuclear current tensor $W(\lambda\lambda')$ in the alternative $(\lambda\lambda')$ form, i.e., those connected with the component $\lambda=0$ and/or $\lambda'=0$, employing current conservation according to Eq. (2.12b) and using

$$\begin{aligned}W^{\lambda\lambda'}=&\left[\sqrt{-\frac{Q^2}{\boldsymbol{Q}^2}}\delta_{\lambda 0}+(1-\delta_{\lambda 0})\right]\\&\times\left[\sqrt{-\frac{Q^2}{\boldsymbol{Q}^2}}\delta_{\lambda' 0}+(1-\delta_{\lambda' 0})\right]W(\lambda\lambda').\end{aligned} \tag{A11}$$

When calculating the nuclear current tensor $W^{\lambda\lambda'}$ in the form (A11), all zero components are to be obtained from the charge matrix element $\langle\psi_\alpha^{(-)}(\boldsymbol{q}_f)\nu_{\alpha_f}(Nd)|j^0(\boldsymbol{p}_N+\boldsymbol{p}_d-\boldsymbol{p}_B,\boldsymbol{p}_N+\boldsymbol{p}_d+\boldsymbol{p}_B)|Bn_B\rangle$ directly instead of from the four-vector current component along the polarization vector $\varepsilon^\mu(Q0)$. With respect to zero components the kinematic and frame-dependent factor $\sqrt{-Q^2/\boldsymbol{Q}^2}$ is split off from the Lorentz-scalar components $W(\lambda\lambda')$; thus, the components of the nuclear current tensor $W^{\lambda\lambda'}$ lost the property of being Lorentz scalars.

In terms of the nuclear current tensor $W^{\lambda\lambda'}$, the contraction $L\cdot W$ takes the final form

$$L \cdot W = v_0 \Bigg[\sum_{\alpha} v_{\alpha}(Q,\theta_e) R^{\alpha}(\boldsymbol{p}_N \boldsymbol{p}_d \boldsymbol{p}_B; n_B) + h_e \sum_{\alpha'} v_{\alpha'}(Q,\theta_e) R^{\alpha'}(\boldsymbol{p}_N \boldsymbol{p}_d \boldsymbol{p}_B; n_B) \Bigg], \quad \text{(A12)}$$

with the kinematic factors defined in Eqs. (2.14a) and the nuclear responses defined in Eqs. (2.15). The contraction $L \cdot W$ is a Lorentz scalar, whereas the nuclear responses in general are not. The actual calculation of this paper will use the lab frame with $\boldsymbol{p}_B = \boldsymbol{0}$ for the nuclear responses.

[1] H. Meier-Hajduk, U. Oelfke, and P.U. Sauer, Nucl. Phys. **A499**, 637 (1989).
[2] R.W. Schulze and P.U. Sauer, Phys. Rev. C **48**, 38 (1993).
[3] K. Chmielewski, diploma thesis, University of Hannover, 1993.
[4] R.-W. Schulze and P.U. Sauer, Phys. Rev. C **55**, 1051 (1997).
[5] U. Oelfke, P.U. Sauer, and F. Coester, Nucl. Phys. **A518**, 593 (1990).
[6] E.v. Meijgaard and J.A. Tjon, Phys. Rev. C **42**, 74 (1990); **42**, 96 (1990); **45**, 1463 (1990).
[7] H. Kamada, W. Glöckle, and J. Golak, Nuovo Cimento Soc. Ital. Fis., A **105A**, 1435 (1992).
[8] J. Golak, H. Kamada, H. Witała, W. Glöckle, and S. Ishikawa, Phys. Rev. C **51**, 1638 (1995).
[9] L.P. Yuan, K. Chmielewski, M. Oelsner, P.U. Sauer, A.C. Fonseca, and J. Adam, Jr., Nucl. Phys. **A689**, 433c (2001).
[10] L.P. Yuan, K. Chmielewski, M. Oelsner, P.U. Sauer, A.C. Fonseca, and J. Adam, Jr., Few-Body Syst. **32**, 83 (2002).
[11] S. Nemoto, K. Chmielewski, J. Haidenbauer, S. Oryu, P.U. Sauer, and N.W. Schellingerhout, Few-Body Syst. **24**, 213 (1998).
[12] S. Nemoto, K. Chmielewski, J. Haidenbauer, U. Meyer, S. Oryu, and P.U. Sauer, Few-Body Syst. **24**, 241 (1998).
[13] K. Chmielewski, S. Nemoto, A.C. Fonseca, and P.U. Sauer, Few-Body Syst., Suppl. **10**, 335 (1998).
[14] J. Adam, Jr., F. Gross, S. Jeschonnek, P. Ulmer, and J. Van Orden, nucl-th/0204068.
[15] T.W. Donnelly and A.S. Raskin, Ann. Phys. (N.Y.) **169**, 247 (1986).
[16] V. Dmitrasinovic and F. Gross, Phys. Rev. C **40**, 2479 (1989).
[17] M. Lacombe, B. Loiseau, J.M. Richard, R. Vinh Mau, J. Coté, P. Pirès, and R. de Tourreil, Phys. Rev. C **21**, 861 (1980).
[18] C. Hajduk, P.U. Sauer, and W. Strueve, Nucl. Phys. **A405**, 581 (1983).
[19] M. Gari and W. Krümpelmann, Phys. Lett. B **173**, 10 (1986).
[20] W. Strueve, C. Hajduk, P.U. Sauer, and W. Theis, Nucl. Phys. **A465**, 651 (1987).
[21] P.H.M. Keizer, Ph. D. thesis, University of Amsterdam, 1986; E. Jans (private communication).
[22] E. Jans *et al.*, Nucl. Phys. **A475**, 687 (1987).
[23] C.M. Spaltro *et al.*, Phys. Rev. Lett. **81**, 2870 (1998).
[24] C.M. Spaltro *et al.*, Nucl. Phys. **A706**, 403 (2002).
[25] D. W. Higinbotham *et al.*, JLab Hall: A approved-proposal 02-108; (private communication).